3 Aerosol Flux Measurement System

3.1 Introduction

This chapter begins with an account of the need for modification of a CPC for use in making flux measurements. The design of the UMIST CPC flux measurement system is then outlined, and outline accounts are given of the logging and analysis software written for the system.

3.1.1 Necessity for Measuring Fluxes Using a CPC

It is important to be able to measure aerosol fluxes in order to quantify the effects of aerosol on a given landscape, to measure rates of aerosol production and to understand aerosol transport. The eddy covariance method (chapter 2) is a possible means of performing these measurements, however aerosol has traditionally been one of the more problematic species to study using this method. This is due to counting statistical limitations (chapter 2) and because there have until recently been no attempts made to modify existing instruments to rapidly measure concentrations of aerosol smaller than 100 nm.

Aerosol instruments used in the past have generally been optical sizing probes (ASASP-X, FSSP, ASASP-555-X *etc.*, Droplet Measurement Technologies, Boulder, Colorado). These all use Mie scattering theory to determine the diameter of aerosol observed (scattering intensity, $I = f(D_p)$). However, all the probes listed above use (red) visible light to count and size aerosol. This means that in "normal" dry deposition study conditions (typically rural sites) fluxes can only be calculated for a relatively narrow diameter range. The lower limit of this range is around 100 nm and is a result of the lack of scattering from aerosol with diameters similar to the wavelength of light used. The upper limit is dependent on the ambient aerosol size distribution, but it was found in this study that statistical requirements made it impossible to reliably calculate fluxes of aerosol larger than around 1 – 1.5 μm in

rural conditions. This is due to the low flow rate of the ASASP-X used (2 cm^3 s^{-1}) and the low number concentrations of these large particles normally observed.

There are several types of instrument capable of counting sub–100 nm aerosol. Notably, systems exist in which Faraday cups are connected to pico-ammeters (e.g. Fontan *et. al.*, 1997). Although the use of such a detection system was investigated, the technique was rejected because of the need for the use of size distribution measurements to infer the relationship between measured current and aerosol concentration. Other difficulties inherent in this approach include the cost of sufficiently accurate ammeters and the difficulty in avoiding this cost by constructing pico-ammeters which do not suffer from excessive noise. Instead, here a modified single particle detection method has been used. The detector used was a Condensation Particle Counter (CPC). Much of the work presented here is based on fine aerosol flux measurements made using a specially adapted CPC. The following sections describe the operation of CPCs and modifications made to produce the UMIST CPC Flux System.

3.2 Principles of the Condensation Particle Counter

The basic operation of the CPC is the same as that of the size resolving probes listed above. A particle passes through a beam of light and scatters the light. The scattering is detected and the particle is counted. Given a known flow rate, the number of particles detected in a given time interval can be divided by the volume of air "scanned" and a number concentration calculated. Unlike size resolving probes, the intensity of scattering is *not* recorded by a CPC, and it is this intensity which can be used to determine particle diameter using Mie theory. So, CPCs only measure *total number concentration* for their operating diameter ranges.

There are several types of CPC available. The counter used in this study (and represented in figure 1) was a non-isothermal continuous flow diffusion CPC. In this type of instrument, incoming aerosol are mixed with a saturated butan-1-ol vapour (in the saturator), then the sample stream is cooled (in the condenser) to supersaturate the mixture with respect to butane. This causes the particles to grow by condensation to a detectable diameter. The concentration is then determined by single particle counting in the detection chamber, giving an accurate, calibration free determination of the absolute number concentration.

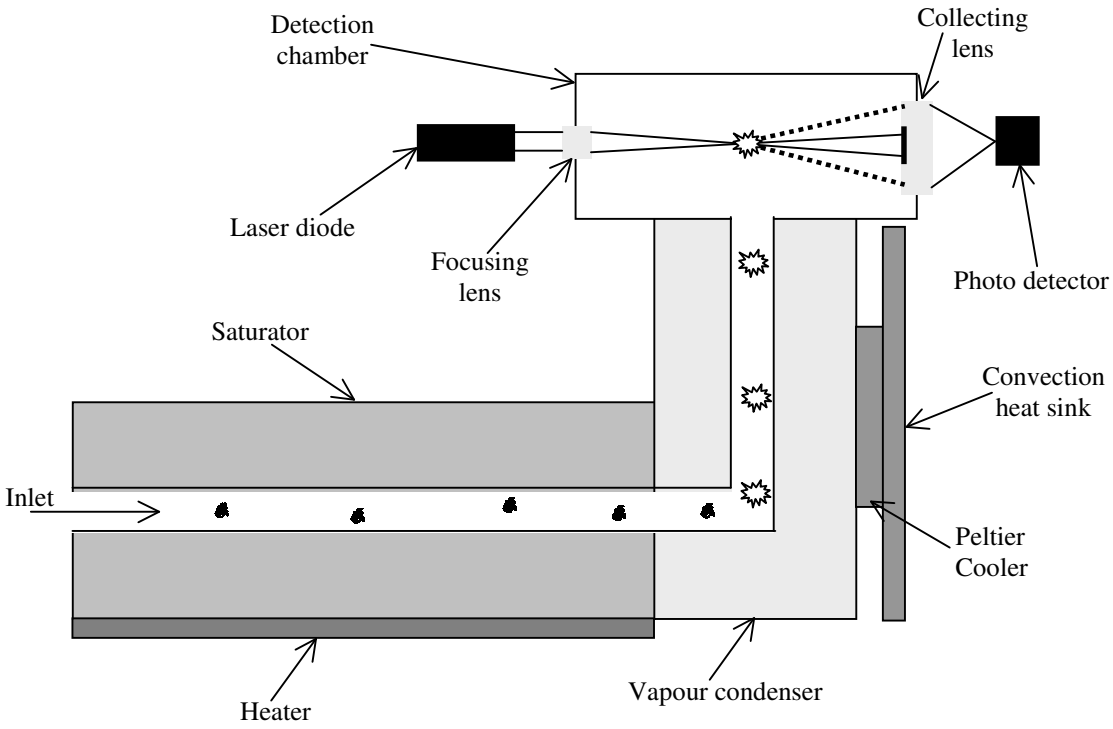

Figure 1. Schematic diagram of the operation of a CPC. The saturator mixes the incoming aerosol with Butan-1-ol saturated air. The mixture is cooled in the condenser so that the butane vapour pressure is above saturation, – particles grow to a detectable size in the condenser, and are then counted in the detection chamber.

Studies on the operation and diameter dependent counting efficiency of many different types of CPCs have been published recently. Ankilov et. al. (2002) compare the efficiency of ten different instruments (four adiabatic expansion counters, three continuous flow diffusion counters and three turbulent mixing counters) and find that the 50% detection efficiency cut-off of the flow diffusion type instruments are as quoted by their manufacturer (TSI Inc., St. Paul, Michigan, USA). Mavliev (2002) goes into significantly more detail on the theory behind particle growth for a turbulent

mixing CPC, while Sem (2002) studies the detection efficiency of three non-isothermal continuous flow diffusion CPCs manufactured by TSI, again finding the manufacturer's quoted lower diameter cut-off figures accurate.

The instrument used in this study was a TSI 3760-A condensation particle counter. Although there are no detailed studies on this particular counter in the literature, the investigations above, of very similar counters by the same manufacturer (3022-A, 3025-A and especially the 3010) show satisfactory response to small particles. The cut-off for the 3760-A CPC is 11 nm. This means that 50% of all 11 nm particles entering the instrument are counted. Because the counting efficiency of these instruments around the lower detection limit behaves similarly to the left hand half of a bell curve, it is reasonable to quote 11 nm as the lower detection limit in the case of the 3760-A.

3.3 Flux measurement using a CPC

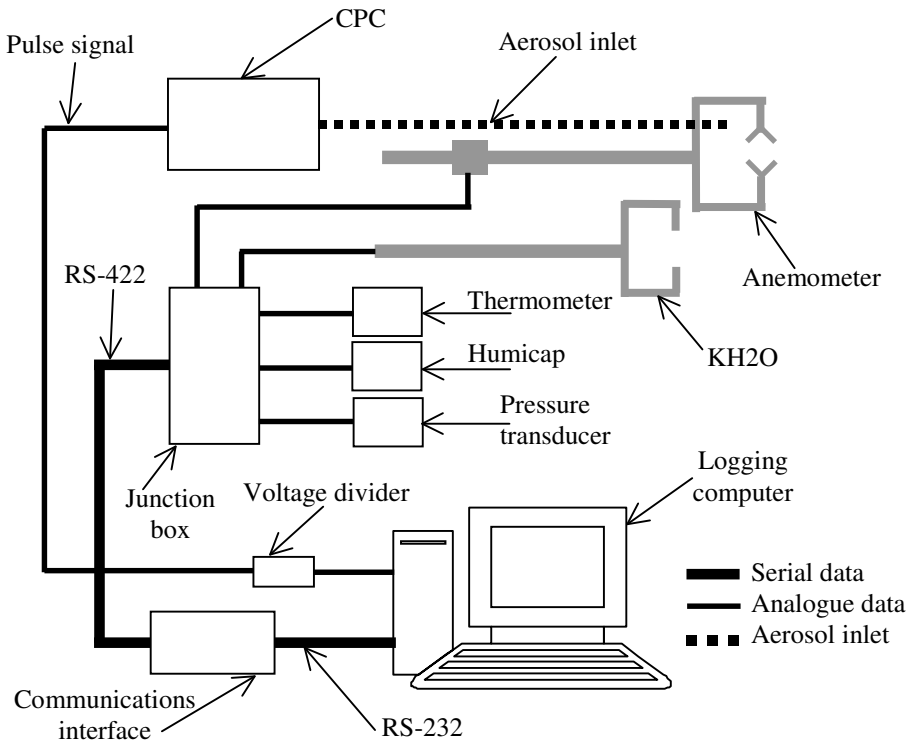

Figure 2. Schematic diagram of the UMIST CPC flux measurement system. See key (lower right) for data connection types. Item labelled "Junction box" contains the system's analogue to digital converters.

As outlined in chapter 2, eddy covariance aerosol flux measurements rely on the resolution of fluctuations in aerosol concentration and vertical wind speed in pseudo-real time. This places demands on the temporal response of the aerosol sensor used. In this chapter, it will be assumed that the response of the TSI 3760-A is adequate for making flux measurements in general. The actual response of the counter and the effect of this on the reliability of calculated fluxes will be addressed on a case-by-case basis where such results are presented (chapters four and six). It is enough to note here that the counter frequency response does not significantly limit the validity of any of the results presented in this thesis, as determined by spectral analysis of the relevant time series.

The use of the CPC to measure fluxes was relatively straightforward. The 3760-A can be configured to produce a 6-volt pulse when a particle is detected. This is, in fact, the amplified output of the photo-detector. These pulses were sent to a National Instruments PCI-6601 event counter card (National Instruments, Austin, Texas, USA) installed in the logging computer, via a 100 m, 50 Ω coaxial cable. A Gill HS sonic anemometer (Gill Instruments, Lymington, UK) was used to measure wind speed, this data being logged by the same computer via a serial connection. Other sensors, including a pressure transducer (Vaisala PTB 100, Vaisala, Helsinki, Finland), relative humidity and temperature sensor (Humicap HMP 50 Y, Vaisala, Helsinki, Finland), second Platinum resistance thermometer (PRT 100 type) and a fast response water vapour sensor (KH2O; Campbell Scientific Inc., Loughborough, UK) were logged using analogue to digital converters supplied with the anemometer.

Figure 2 shows, schematically the sensors used and their and data connections. Power connections are not shown in the interest of clarity. Chapter four contains a photograph of the system as deployed during the GRAMINAE integrated experiment. Having outlined the structure of the system, the following sections describe the custom logging and analysis software, and the calculations involved in the flux calculations as implemented in this system.

3.4 CPC Flux system software

The hardware used in the UMIST CPC flux system (see diagram above) is in general, "off the shelf". The only custom-built data critical components were the voltage divider (to avoid voltage overloading of the event counter card), the logging computer, and the logging and analysis software. Development of these two distinct software components comprised the most significant task in both the design and implementation of the system.

Although CPCs have been used in the past (most significantly by Buzorius *et. al.*, 1998) to measure aerosol fluxes, the UMIST system took advantage of the single particle counting operation of this type of CPC to remove any possible system induced frequency dependence except that of the CPC itself. The arrangement described by Buzourius *et. al.* (1998, 2000) relied upon a frequency to voltage converter to approximate the number of aerosol detected to an analogue voltage for logging by conventional means. The guiding design principle behind the system described here was optimisation of frequency response, because of doubts about the adequacy of CPCs for flux measurement (chapters two and four). Because of the perceived need to resolve individual particle detections, and the use of an event counting card to facilitate this, custom written logging software was required. The following sections describe, respectively, the logging and analysis software.

3.4.1 Logging software

The primary task of the logging software was to set up the sonic anemometer and to log serial data from the anemometer. In the software version used to gather the data included in this thesis, the logging computer polled its own first two serial ports at each of the seven most common Baud rates used by the HS anemometer (2400 – 115200 Baud). On detecting an active anemometer the screen shown below (figure 3) was presented, giving options for data formatting, header file definitions and reporting rates.

The options screen shown in figure 3 displays the detected anemometer configuration (serial port number and current Baud rate), configures the file output format, the contents of the header files (written each time the software is restarted), the calculated required Baud rate (given the requested data acquisition rate) and the anemometer reporting rate. It also passes the report rate to the next stage of the logging software.

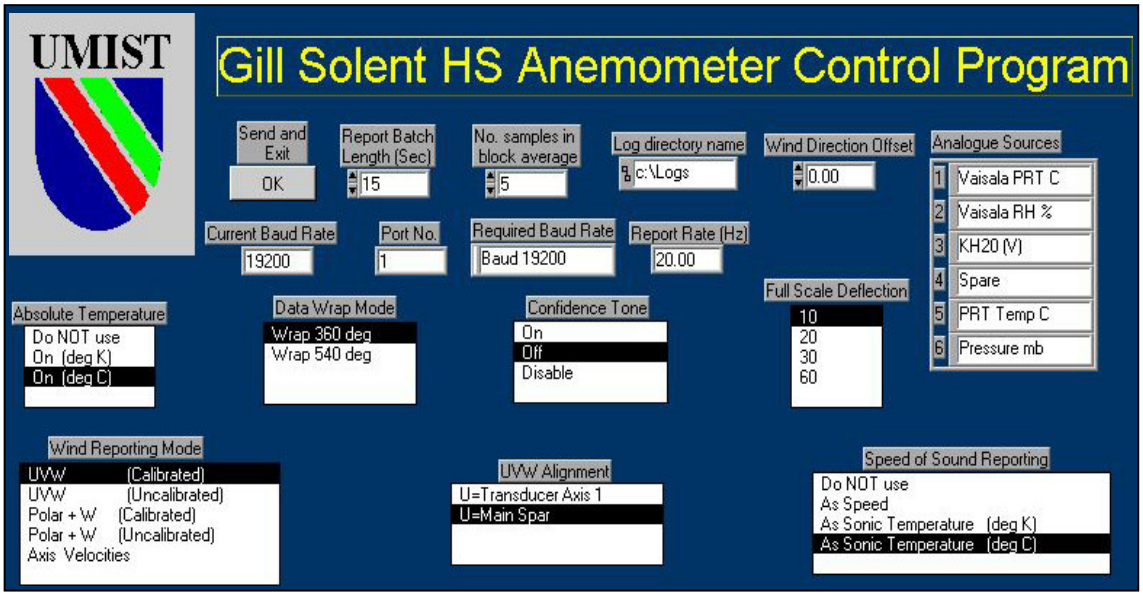

Figure 3. Initial anemometer set-up menu from the UMIST CPC system software. Entries shown are default values.

Here the event counter card is initialised. This happens in three stages, which are most easily explained in conjunction with details of the mode of operation of the counter in this application.

Because of the relatively high rate of data acquisition with the system described, software timed polling of the event counter was not reliable. In order to calculate aerosol number concentration rapidly enough to subsequently derive fluxes under certain circumstances, it was necessary to read the accumulated number of pulses at 20 Hz. It was found that using software timed polling (where the logging software must send a request to the event counter via the PCI bus) the interval between subsequent polls could not be controlled to better than 0.01 seconds. This introduced a random variability of 20% of the total concentration into the aerosol time series at 20 Hz.

In view of these limitations, the event counter was set up to time its own counting intervals using an accurate on-board hardware clock. The PCI-6601 has several pulse

generators, one of which was wired into the circular buffer timer of the counting channel. Accordingly, the first of the three above mentioned steps in the initialisation of the event counter was to set up the trigger channel to generate a square wave with a duty cycle of 10% at a user definable frequency, – the acquisition rate (normally 20 Hz). This was controlled by the "Report batch length" option, – figure 3, where the batch length is the number of 100 Hz reports to average into each recorded datum (*e.g.* 5 for 20 Hz). The second step was to set up the circular data buffer on the counter card. This was the intermediate data storage location, in between hardware timed data acquisition and software timed logging to the hard disc. Finally, the buffer was cleared and acquisition commenced.

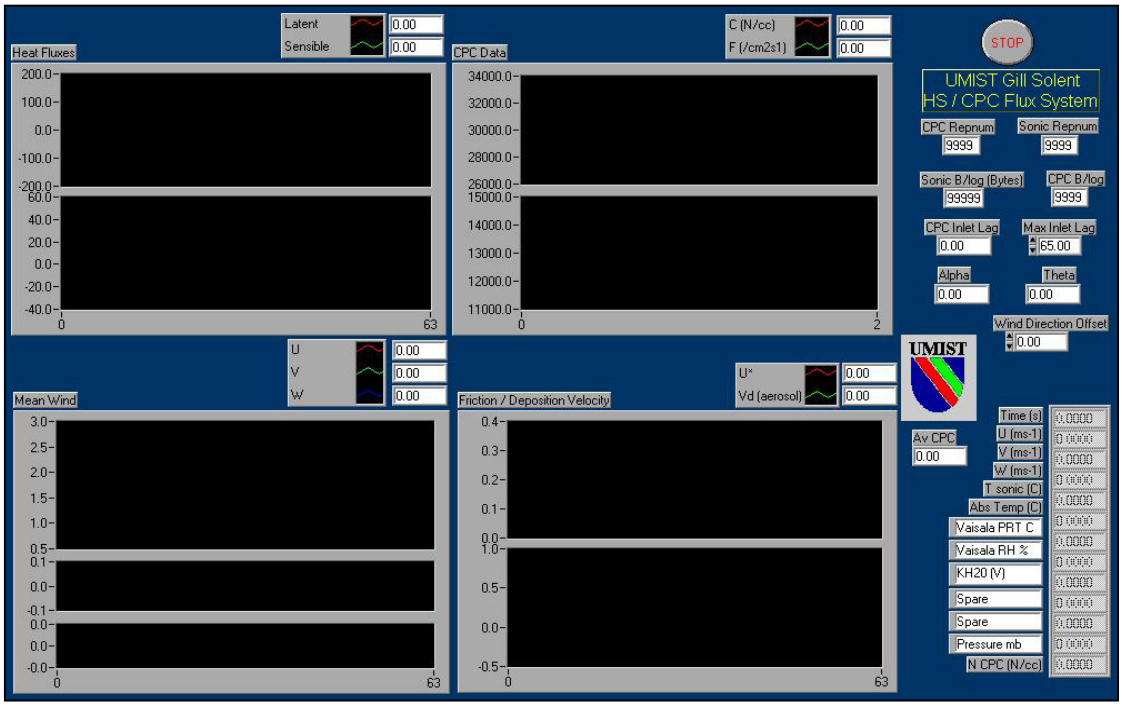

Figure 4. Screen shot of the logging window. Values shown are defaults. Charts display values calculated over a 15-minute averaging period.

At the same time, the serial buffer was cleared, to synchronise the data from the anemometer with that from the CPC. This marked the end of the logging software set-up phase. The logging window was automatically launched at this point. Data was written to the hard drive at a user definable rate, normally every 15 seconds, as a compromise between keeping computational overhead low and storing data regularly enough that losses would be minimal in the event of a power or operating system

failure. Data were logged in arrays of binary numbers, the exact format being determined by the sizes and accuracy of the numbers themselves.

Other options visible in figure 3 include the analogue channel names for the header file to allow simple identification of each channel at a later date, the directory to log data to and the wind direction offset (to correct wind direction data for the direction of the anemometer). Other options were the speed of sound reporting mode (as temperature in °C or K) or as speed, the wind direction wrapping (to 360° or 540°), the alignment of the anemometer co-ordinate system and whether to operate the "Confidence Tone", – a high pitched tone indicating proper operation of the anemometer.

Figure 4 shows a screen shot of the logging window. The series of digital indicators in the lower right corner of the window display average values for each channel at 1 Hz. "CPC Repnum" and "Sonic Repnum" show the number of reports read from the event counter card and the anemometer respectively (as a run-time check, this should always be equal to the logging rate). "CPC B/log" and "Sonic B/log" showed the amount of un-recovered data in the counter card and serial port buffers. Either of these indicators taking on a high value was an indication of some kind of problem with the acquisition system, and also a warning that the recorded time series may not be co-incident.

Other indicators included the parameters and results for the calculation of the inlet lag time for the CPC, the calculated rotation angles (chapter 2), and chart displays of wind speed, u_*, aerosol deposition velocity v_d, aerosol concentration and flux, and latent and sensible heat fluxes all calculated online over a 15 minute period. The calculations were performed in a similar manner to those included in the post-processing software, to be described in the next section. These preliminary calculations were included to give confidence that the logged data produced reasonable results, while there was still the opportunity to correct any system faults (in the field).

3.4.2 Flux calculation software

A separate, independent software application was written to calculate fluxes and other micrometeorological parameters from the logged raw data files. Because this was a rather large and complicated application, the simplest way to gain an impression of its operation is the diagram shown as figure 5.

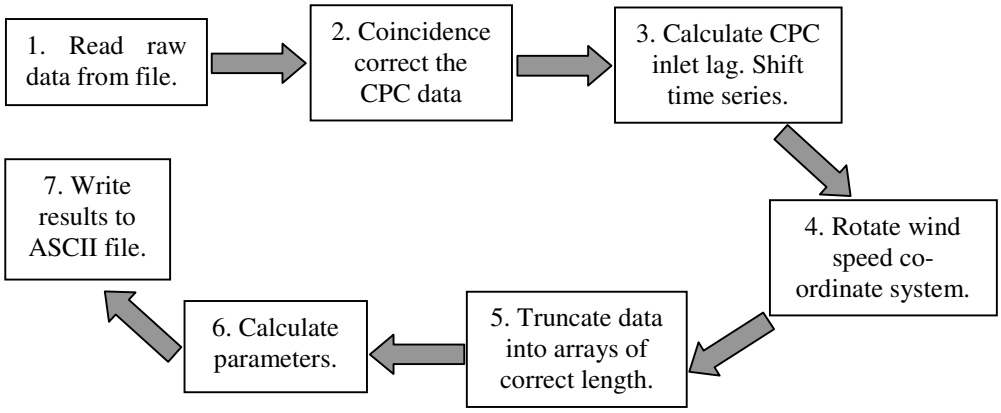

Figure 5. Flow diagram showing the stages involved in calculating fluxes and micrometeorological parameters from CPC flux system data.

Here the seven stages of the analysis procedure are shown. The first ("Read raw data from file") is straightforward. It involves queuing the one hour data raw data files from the logging software, removing fragments of files (those containing less than 15 minutes' data), reading the data from the first hour's file, stripping out the un-needed time series (*e.g.* the second platinum resistance thermometer channel, floating analogue channels) and passing the values to stage two of the software. This first phase of the analysis controls the execution of the rest of the application, in that it starts and ends the flow of data, and determines which data are analysed.

Stage two of the analysis is a correction for counting co-incidence errors, performed on the full one-hour files. The correction is presented as equation 3.1, and is taken from the operation manual for the TSI CPC 3760-A. It is simply an exponential function, which describes the probability of more than one Butanol grown particle passing through the detecting laser beam at the same time:

$$\chi_c = \chi \cdot e^{\chi \times 10^{-5}} \qquad (3.1)$$

where χ_c is the co-incidence corrected aerosol concentration and χ is the uncorrected (logged) concentration.

Stage three of the process is calculation of the CPC inlet lag time. This is the time taken for aerosol to enter the inlet near the anemometer transducers, be drawn down the inlet tube and be detected. The lag time is determined using the cross correlation between aerosol concentration and vertical wind speed. This is calculated according to:

$$r_{w\chi} = \int_{-\infty}^{\infty} w(t) \cdot \chi(t+\tau) dt \qquad (3.2)$$

where $w(t)$ is the vertical wind speed time series and $\chi(t+\tau)$ is the aerosol concentration series shifted relative to the first series by time τ. The factor τ is varied between zero and a user defined maximum value, normally set to twice the expected lag time. The lag time is defined in the software as the value of τ where $r_{w\chi}$ is at its maximum value, – *i.e.* where the correlation between w and χ is highest. Having determined the lag time, the aerosol concentration time series is shifted relative to the w series by τ seconds, so that during the rest of the analysis, correlated variations in w and χ coincide in the time series.

The fourth phase of the operation outlined in figure 5 is the co-ordinate system rotation, defined and explained in chapter 2. Following this, the array of data is split into smaller arrays according to the averaging time required. In the case of work presented here, this period was always 15 minutes, – so the one hour data files were split into four equal arrays.

The sixth stage of the data analysis was to calculate fluxes and meteorological parameters for the prepared, split arrays produced by the first five operations. Fluxes were determined using the equations presented in chapter 2, and standard deviations for all rapidly measured quantities were determined. Finally, the results of the analysis

were written to an ASCII file, for later examination (usually in a spreadsheet). This marks the end of the routine data analysis procedure. However, further software tools were developed to assist in visualisation and interpretation of data generated by the system.

3.4.3 Fourier analysis tools

A third associated application was developed to run Fourier analyses on the data gathered by the flux measurement system. This was largely based on the flux calculation software, but rather than calculating fluxes it produced small binary files containing frequency averaged power and co-spectral transforms for each fifteen minute period, normalised by variance or co-variance respectively. This too used the definitions given in chapter 2 for these types of analyses.

Yet another program was written to conditionally average the transform files according to parameters such as boundary layer stability, aerosol flux or heat flux *etc.* It was this program which generated the power and co-spectral data presented in this thesis.

3.4.4 Data visualisation

Finally, an analysis routine was written to conduct quadrant analyses on the data. Again, this technique is outlined in chapter 2, and results are presented in the section on urban micrometeorology.